applied sciences

MDPI

Article

Artificial Neural Network (ANN) Validation Research: Free Vibration Analysis of Functionally Graded Beam via Higher-Order Shear Deformation Theory and Artificial Neural Network Method

Murat Çelik [1,*], Emircan Gündoğdu [2], Emin Emre Özdilek [1], Erol Demirkan [1] and Reha Artan [1]

[1] Department of Civil Engineering, Istanbul Technical University, 34469 Istanbul, Turkey; artanr@itu.edu.tr (R.A.)
[2] Department of Computer Engineering, Istanbul Technical University, 34469 Istanbul, Turkey
* Correspondence: celikmur15@itu.edu.tr

Abstract: Presented herein is the free vibration analysis of functionally graded beams (FGMs) via higher-order shear deformation theory and an artificial neural network method (ANN). The transverse displacement (w) is expressed as bending (w_b) and shear (w_s) components to define the deformation of the beam. The higher-order variation of the transverse shear strains is accounted for through the thickness direction of the FGM beam, and satisfies boundary conditions. The governing equations are derived with the help of Hamilton's principle. Non-dimensional frequencies are obtained using Navier's solution. To validate and enrich the proposed research, an artificial neural network method (ANN) was developed in order to predict the dimensionless frequencies. Material properties and previous studies were used to generate the ANN dataset. The obtained frequency values from the analytical solution and ANN method were compared and discussed with respect to the mean error. In conclusion, the solutions were demonstrated for various deformation theories, and all of the results were thereupon tabularized and visualized using 2D and 3D plots.

Keywords: functionally graded material; composite beam; artificial neural network; free vibration

check for updates

Citation: Çelik, M.; Gündoğdu, E.; Özdilek, E.E.; Demirkan, E.; Artan, R. Artificial Neural Network (ANN) Validation Research: Free Vibration Analysis of Functionally Graded Beam via Higher-Order Shear Deformation Theory and Artificial Neural Network Method. *Appl. Sci.* **2024**, *14*, 217. https://doi.org/10.3390/app14010217

Academic Editor: Alberto Corigliano

Received: 13 November 2023
Revised: 21 December 2023
Accepted: 24 December 2023
Published: 26 December 2023

1. Introduction

Functionally graded materials (FGMs) are composite materials with advanced and programmable structures whose physical and mechanical properties can vary in different directions. Recently, with the major technological breakthroughs made in fields such as materials engineering and artificial intelligence (AI), the design and optimization of FGMs have come into prominence with great momentum. Substantial investments made in the past few decades, especially in areas such as materials and software engineering, have recently begun to bear fruit. In this context, the importance of functional materials created using smart materials has increased considerably in fields such as energy, electronics, aircraft and space engineering, construction, and defense. To be more precise, a good analysis of such functional materials will maximize the efficiency of the designed engineering structure. Undoubtedly, functionally graded materials (FGMs) have an important place among the mentioned materials.

FGMs have significant potential in the analysis of composite materials, with their unique physical and mechanical properties. Functional materials are generally obtained by combining two different materials that have a certain harmony between them. These are often composite structures designed in ceramic–metal or ceramic–polymer forms, with smooth transitions from one surface to another.

Although there are many different methods for analyzing functional materials, the most prominent are Euler–Bernoulli beam theory (CBT), Timoshenko beam theory (first-order shear deformation theory), higher-order shear deformation theories, and nonlocal approaches. First-order shear deformation theory takes into account the shear effect, which is ineffective in CBT. The existence of advanced theories that consider shape factor, which arises depending on the geometry of the composite material and allows us to calculate the deformation most accurately, has turned research towards higher-order theories. Hence, the need for enhanced theories has become inescapable. To avoid the use of the shear correction factor and to better predict the behavior of FGM beams, third-order shear deformation theories [1,2], sinusoidal theory [3], and hyperbolic deformation theory [4] have been proposed. Using various higher-order shear deformation beam theories, bending and free vibration analyses of functionally graded beams are developed [5].

In the present study, the free vibration behavior of an FG beam is analyzed via both higher-order shear deformation theory and artificial neural network (ANN) methods. The ANN method is a kind of AI method that allows advanced algorithms to accurately predict material behavior. Owing to this cutting-edge method, the computational time is also considerably reduced. Looking back over the past decade, machine learning, the latest trend in computer systems, has attracted great attention. The main reason for this is that thanks to this system, dynamic data can be stored, interpreted, and, most importantly, easily integrated into science and industry. Moreover, current studies have shown that thanks to this technology, engineering applications and problems can be tested and interpreted very quickly. In this way, free vibration frequencies can easily be tested for different deformation theories in research.

First, a mathematical model is proposed using higher-order shear deformation theory (HSDT). Then, kinematic relations and constitutive equations are obtained using Hamilton's law. The analytical solution is performed for simply supported boundary conditions. Then dimensionless frequencies are attained using Navier's solution procedure. To validate and enrich the present research, an ANN method was developed and trained using material properties data obtained from previous studies. Recently, the researchers of [6] studied nonlocal FGM nanoplates using higher-order isogeometric analysis and the ANN method to predict free vibration behavior. They demonstrated that the obtained values from the ANN converged with a considerable margin of error compared to the analytical solution.

Reddy [7] carried out studies involving linear and nonlinear theories to examine the deformations and stresses of functionally graded plates. Vel and Batra [8] studied the deformations of an FGM plate pinned from both ends in a mechanical and thermal environment by comparing different deformation theories. Ferreira et al. [9] analyzed the behavior of a simply supported functionally graded plate using a third-order shear deformation theory. Neves et al. [10] presented the sinusoidal shear deformation theory for vibration analysis of a functionally graded element. Taj et al. [11] conducted a series of analyses of FG plates with an effective °C iso-parametric Lagrangian finite element with multiple degrees of freedom for each node, using higher-order deformation theory.

Li [12] investigated the static bending and free vibration behaviors of Timoshenko and Euler–Bernoulli FGM beams using shear deformation and Timoshenko beam theories. Huang and Li [13] studied the free vibration model of axially graded non-uniform beam cross-sections with the help of Fredholm integral equations. Aydoğdu and Taşkın [14] analyzed the free vibration behavior of a simply-supported FGM beam for different deformation theories using a Navier-type solution method. Mahi et al. [15] studied the free vibration behavior of temperature-dependent FGM beams.

Sankar [16] presented elasticity solutions to the bending of Euler–Bernoulli FGM beams. Zhang and Yu [17] studied an analytical solution that analyzes the behavior of beams subjected to mechanical loading with the Airy stress function. Shahrjerdi et al. [18] studied the behavior of functionally graded solar panels under stress using a second-order shear deformation theory. Bending and buckling behaviors of bi-directional Euler–Bernoulli and Timoshenko beams using the strain gradient elasticity and nonlocal elasticity methods were presented in studies [19–21].

Although the analytical solutions of functionally graded composites converge very precisely, the mechanical calculations of such advanced composite structures impose a significant computational load. However, in cases where thermal change and other dynamic effects occur together, the solution to the problem becomes more difficult. ANN methods provide us with a significant guide at this point. The ANN model converges to an outcome with a tolerance of 10^{-4} within a second. This computational efficiency outperforms analytical solutions in terms of time, and with a low tolerance.

There are very few studies in the literature that analyze free vibration, post-buckling behavior, etc. Other effects of advanced composite structures are under different mechanical and environmental conditions. In such situations, validating the research becomes grueling. When artificial intelligence is well-trained, it can be a crucial source for us to check the accuracy of the analysis, and also allows the development of advanced methods by other researchers. In addition, the ANN method offers us many advantages such as optimization of composite structures and estimating appropriate dimensions and material parameters for minimum deformation of the structure in the problem.

The present study offers a new perspective and approach to the traditional methods used in solving such problems in the literature. In view of the current research, recent breakthroughs made in computer engineering and their applied science studies with other disciplines have shown that the machine learning approach is shaping our future daily in terms of material optimization and advanced structural analysis. From this point on, it is noticeable that there is a deficiency in the literature on machine learning-based studies such as ANN approaches.

2. Theory and Formulation

2.1. Material Properties

For a ceramic–metal FGM beam (see Figure 1) having a length L, width b, and thickness h, the geometry of the beam, its material properties, and volume fraction are expressed in Equations (1)–(3). Considering the rule of mixture, the effective material properties P can be written in terms of volume fraction, as shown below:

$$P(z) = P_m V_m + P_c V_c \tag{1}$$

where P_m, P_c, V_m, and V_c denote the material properties of the metal and ceramic associated with the given subindices, respectively.

$$V_m + V_c = 1 \tag{2}$$

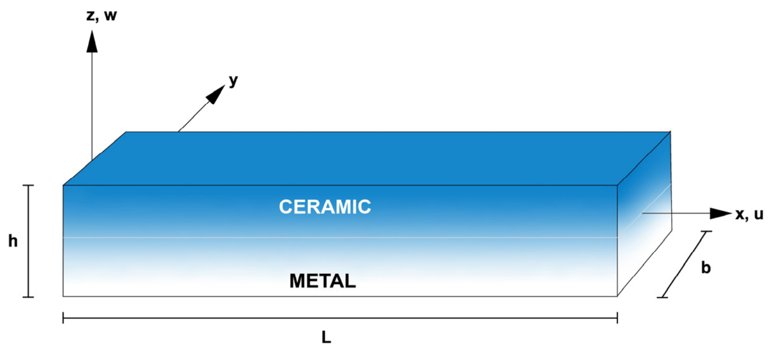

Figure 1. FGM beam.

Note that the distribution of the power law for the volume fraction of ceramic material can be expressed as follows:

$$V_c = \left(\frac{z}{h} + \frac{1}{2}\right)^p \tag{3}$$

where p, which is a number greater than zero, takes a value in the range $0 \leq p \leq \infty$ and is called the power law index. In the case of p = 0, the material becomes fully ceramic.

Considering the above relationship, the material properties in terms of Young's modulus and mass density, as shown below:

$$
\begin{aligned}
E(z) &= E_m + (E_c - E_m)V_c \\
\rho(z) &= \rho_m + (\rho_c - \rho_m)V_c
\end{aligned} \tag{4}
$$

Poisson's ratio is assumed to be constant in our study.

2.2. Constitutive Equations

The displacement field for the higher-order deformation theory can be written in a general form. In this analysis, the transverse displacement w is expressed as the summation of bending (w_b) and transverse (w_s) displacements, as shown below:

$$u(x,z,t) = u_0(x,t) - z\frac{\partial w_b}{\partial x} - f(z)\frac{\partial w_s}{\partial x} \tag{5}$$

$$w(x,z,t) = w_b(x,t) + w_s(x,t) \tag{6}$$

In the present study, the following shape function *f(z)* is chosen based on the hyperbolic function proposed by Soldatos [4]:

$$f(z) = z - \left[h\left(\sinh\left(\frac{z}{h}\right)\right) + z\left(\cosh\left(\frac{1}{2}\right)\right)\right],\ g(z) = 1 - f'(z) \tag{7}$$

The non-zero linear strains derived from Equations (5) and (6) are the following:

$$
\begin{aligned}
&\varepsilon_x = \tfrac{\partial u_0}{\partial x} - z\tfrac{\partial^2 w_b}{\partial x^2} - f(z)\tfrac{\partial^2 w_s}{\partial x^2} \\
&\gamma_{xz} = g(z)\ \ \phi \\
&\phi = \tfrac{\partial w_s}{\partial x}
\end{aligned} \tag{8}
$$

Assuming that the material of the FG beam conforms to Hooke's law, the stresses in the beam are expressed as follows:

$$\sigma_x = E(z)\ \ \varepsilon_x, \qquad \tau_{xz} = \frac{E(z)}{2(1+v)}\gamma_{xz} \tag{9}$$

where

$$Q_{11}(z) = E(z), \quad Q_{55}(z) = \frac{E(z)}{2(1+v)} \tag{10}$$

2.3. Equations of Motion

The equations of motion are attained using Hamilton's principle and integrating with respect to the time, as follows [5]:

$$\delta\int_{t_1}^{t_2}(U + V - K)dt = 0 \tag{11}$$

Here, δU, δV, and δK show the virtual variations of the strain energy, potential energy, and kinetic energy, respectively.

The variational strain energy δU can be written as follows:

$$
\begin{aligned}
\delta U &= \int_0^L \int_{-\frac{h}{2}}^{\frac{h}{2}} (\sigma_x \delta\varepsilon_x + \tau_{xz}\delta\gamma_{xz})dz\ \ dx \\
\delta U &= \int_0^L \left[N_x \tfrac{\partial \delta u_0}{\partial x}\ - M_b \tfrac{\partial^2 \delta w_b}{\partial x^2} - M_s \tfrac{\partial^2 \delta w_s}{\partial x^2} + (Q\ \ \delta\phi)\right]dx
\end{aligned} \tag{12}
$$

Thus, the stress resultants N_x, M_b, M_s, and Q are given as follows:

$$\{N_x\} = \int_{-\frac{h}{2}}^{\frac{h}{2}} \sigma_x \ dz, \quad \{M_b\} = \int_{-\frac{h}{2}}^{\frac{h}{2}} z\,\sigma_x \ dz \tag{13}$$

$$\{M_s\} = \int_{-\frac{h}{2}}^{\frac{h}{2}} \sigma_x\, f(z) \ dz \tag{14}$$

$$Q = \int_{-\frac{h}{2}}^{\frac{h}{2}} g(z) \ \tau_{xz} \ dz \tag{15}$$

The work done by the external vertical load q can be expressed as follows:

$$\delta V = -\int_0^L q\delta(w_b + w_s)dx \tag{16}$$

The variational kinetic energy δK can be written as follows [22]:

$$\begin{gathered}
\delta K = \int_0^L \int_{-\frac{h}{2}}^{\frac{h}{2}} \rho(z)\left[\dot{u} \ \ \delta\dot{u} + \dot{w} \ \ \delta\dot{w}\right] dz \ \ dx \\
\delta K = \int_0^L \int_{-\frac{h}{2}}^{\frac{h}{2}} \rho(z)\left[\dot{u} \ \ \delta\dot{u} + \left(\dot{w}_b + \dot{w}_s\right)\left(\delta\dot{w}_b + \delta\dot{w}_s\right)\right] dz \ \ dx \\
\delta K = \int_0^L J_1\left(\dot{u}_0\,\delta\dot{u}_0 + \left(\dot{w}_b + \dot{w}_s\right)\left(\delta\dot{w}_b + \delta\dot{w}_s\right)\right) - J_2\left(\dot{u}_0\frac{\partial\delta\dot{w}_b}{\partial x} + \frac{\partial\dot{w}_b}{\partial x}\delta\dot{u}_0\right) \\
+J_3\left(\frac{\partial\dot{w}_b}{\partial x}\frac{\partial\delta\dot{w}_b}{\partial x}\right) - J_4\left(\dot{u}_0\frac{\partial\delta\dot{w}_s}{\partial x} + \frac{\partial\dot{w}_s}{\partial x}\delta\dot{u}_0\right) + J_5\left(\frac{\partial\dot{w}_b}{\partial x}\frac{\partial\delta\dot{w}_s}{\partial x} + \frac{\partial\dot{w}_s}{\partial x}\frac{\partial\delta\dot{w}_b}{\partial x}\right) + J_6\left(\frac{\partial\dot{w}_s}{\partial x} + \frac{\partial\delta\dot{w}_s}{\partial x}\right)dx
\end{gathered} \tag{17}$$

If the variational expressions of δU, δV, and δK defined in Equations (12), (16), and (17), respectively, are rewritten into Equation (11), the following equations of motion for the functionally graded beam are obtained:

$$\begin{aligned}
&\delta u_0 \ : \ N'_x = J_1\ddot{u}_0 - J_4\ddot{w}'_s - J_2\ddot{w}'_b \\
&\delta w_b \ : \ M''_b + q = J_1\ddot{w}_b + J_1\ddot{w}_s + J_2\ddot{u}'_0 - J_3\,\ddot{w}''_b - J_5\,\ddot{w}''_s \\
&\delta w_s \ : \ M''_s + Q' + q = J_1\ddot{w}_b + J_1\ddot{w}_s + J_4\ddot{u}'_0 - J_5\,\ddot{w}''_b - J_6\,\ddot{w}''_s
\end{aligned} \tag{18}$$

The inertial coefficients are defined as follows:

$$\{J_1, \ J_2 \ , \ J_3 \ , \ J_4 \ , \ J_5 \ , \ J_6\} = \int_{-\frac{h}{2}}^{\frac{h}{2}} \rho(z)\left(1, \ z, \ z^2, \ f, \ z\,f, \ f^2\right) \ dz \tag{19}$$

By rewriting Equation (18) and considering Equation (19), the equations of motion for the FGM beam can be written as shown below:

$$A_{11}\frac{\partial^2 u_0}{\partial x^2} - B_{11}\frac{\partial^3 w_b}{\partial x^3} - B^s_{11}\frac{\partial^3 w_s}{\partial x^3} = J_1\ddot{u}_0 - J_4\frac{\partial\ddot{w}_s}{\partial x} - J_2\frac{\partial\ddot{w}_b}{\partial x} \tag{20}$$

$$B_{11}\frac{\partial^3 u_0}{\partial x^3} - D_{11}\frac{\partial^4 w_b}{\partial x^4} - D^s_{11}\frac{\partial^4 w_s}{\partial x^4} + q = J_1\left(\ddot{w}_b + \ddot{w}_s\right) + J_2\frac{\partial\ddot{u}_0}{\partial x} - J_3\frac{\partial^2\ddot{w}_b}{\partial x^2} - J_5\frac{\partial^2\ddot{w}_s}{\partial x^2} \tag{21}$$

$$B^S_{11}\frac{\partial^3 u_0}{\partial x^3} - D^S_{11}\frac{\partial^4 w_b}{\partial x^4} - H^s_{11}\frac{\partial^4 w_s}{\partial x^4} + A_{55}\frac{\partial^2 w_s}{\partial x^2} + q = J_1\left(\ddot{w}_b + \ddot{w}_s\right) + J_4\frac{\partial\ddot{u}_0}{\partial x} - J_5\frac{\partial^2\ddot{w}_b}{\partial x^2} - J_6\frac{\partial^2\ddot{w}_s}{\partial x^2} \tag{22}$$

where

$$\left\{A_{11},\ B_{11},\ D_{11},\ B_{11}^S,\ D_{11}^S,\ H_{11}^S\right\} = \int_{-\frac{h}{2}}^{\frac{h}{2}} Q_{11}\left(1,\ z,\ z^2,\ f,\ z\,f,\ f^2\right)\ dz \tag{23}$$

$$A_{55} = \int_{-\frac{h}{2}}^{\frac{h}{2}} Q_{55}\ \left(g(z)\right)^2\ dz \tag{24}$$

3. Solution Procedure

3.1. Analytical Part of Solution

The purpose of Navier's approach is to determine the natural frequency (w) of the FG beam that is simply supported from both ends. The parameters u_0, w_b, and w_s can be expressed by assuming the following expressions [22]:

$$\left\{\begin{array}{c} u_0 \\ w_b \\ w_s \end{array}\right\} = \sum_{m=1}^{\infty} \left\{\begin{array}{c} U_m\ e^{i\,\omega\,t}\cos(\lambda x) \\ W_{bm}\ e^{i\,\omega\,t}\sin(\lambda x) \\ W_{sm}\ e^{i\,\omega\,t}\sin(\lambda x) \end{array}\right\} \tag{25}$$

where the unknown coefficients U_m, W_{bm}, and W_{sm} should be determined; w is the eigenfrequency associated with m^{th} eigenmode, and $\lambda = \frac{m\pi}{L}$.

For the simply supported beam, the boundary conditions are given as shown below [14]:

$$\begin{aligned} & N_x \delta u_0|_0^L = 0 \\ & (M'_s + Q)\delta w_s|_0^L = 0 \\ & (M'_b)\delta w_b|_0^L = 0 \\ & u = w = M_b = 0 \qquad at \qquad x = 0,\quad L \end{aligned} \tag{26}$$

The following q load is considered as in study [5]:

$$q(x) = \sum_{m=1}^{\infty} q_m \sin(\alpha x) \tag{27}$$

$$q_m = \frac{2}{L}\int_0^L q(x)\sin(\alpha x)\,dx \tag{28}$$

$$q_m = \left\{\begin{array}{ll} q_0\ (m = 1) & \text{for sin usoidal load } q_0 \\ \frac{4q_0}{m\pi}\ (m = 1, 3, 5, \ldots) & \text{for uniform load } q_0 \end{array}\right. \tag{29}$$

Substituting the variables u_0, w_b, and w_s from Equation (25) into the equations of motion, Equations (20)–(22), the solutions can be obtained analytically by taking the determinant of the given matrix associated with the components of K_{ij} and m_{ij} [22]. In the present study, q_m is assumed to be zero (q_m = 0).

$$\left(\begin{bmatrix} K_{11} & K_{12} & K_{13} \\ K_{12} & K_{22} & K_{23} \\ K_{13} & K_{23} & K_{33} \end{bmatrix} - \omega^2 \begin{bmatrix} m_{11} & m_{12} & m_{13} \\ m_{12} & m_{22} & m_{23} \\ m_{13} & m_{23} & m_{33} \end{bmatrix}\right)\left\{\begin{array}{c} U_m \\ W_{bm} \\ W_{sm} \end{array}\right\} = \left\{\begin{array}{c} 0 \\ q_m \\ q_m \end{array}\right\} \tag{30}$$

where

$$
\begin{aligned}
&K_{11} = A_{11}\lambda^2, && K_{12} = -B_{11}\lambda^3, && K_{13} = -B_{11}^s\lambda^3, \\
&K_{22} = D_{11}\lambda^4, && K_{23} = D_{11}^s\lambda^4, && K_{33} = H_{11}^s\lambda^4 + A_{55}\lambda^2, \\
&m_{11} = J_1, && m_{12} = -\lambda J_2, && m_{13} = -\lambda J_4, \\
&m_{22} = J_1 + \lambda^2 J_3, && m_{23} = J_1 + \lambda^2 J_5, && m_{33} = J_1 + \lambda^2 J_6
\end{aligned}
\tag{31}
$$

3.2. Artificial Neural Network (ANN) Method

An artificial neural network (ANN) is a computational model that is inspired by the structure and function of biological neural networks in the human brain. It comprises interconnected nodes, known as neurons, organized systematically into layers. These neurons work in harmony to process and transform input data into meaningful output. The configuration of an ANN, in terms of the number of neurons within each layer (i.e., height) and the number of layers (i.e., depth), is a critical factor that influences the network's capacity to perform a given task. In an ANN, data are typically fed into the input layer, and information flows through the network's hidden layers to the output layer. Each connection between neurons is associated with a weight w, which influences the strength of the signal transmitted between neurons. These weights are adjusted during the training process where the network learns to map input data to the desired output. In the present research, it is a supervised learning approach, since we have access to the corresponding outputs for the inputs.

Specifically, all neurons in an ANN receive one or more input values from the previous layer, which are each associated with weights, denoted as $\{x_1, x_2, \ldots, x_n\}$ and $\{w_1, w_2, \ldots, w_n\}$, respectively. Then, a neuron performs $g(\sum_{i=1}^{n} w_i x_i + b)$ with bias b and activation function $g(\cdot)$. Here, the $g(\cdot)$ function introduces nonlinearity into the model, for example, widely used activation functions are sigmoid, tanh, ReLU, and leaky ReLU.

In this study, we aimed to predict $\overline{\omega}$ (i.e., dimensionless frequency) from 4 inputs, which are the beam theory, beam type, *L/h*, and *p*, as shown in Figure 2. Since the first three variables represent categorical values, for instance, *L/h* is drawn from a finite set of {5, 10, 20, 30, 100}, we are encouraged to use a categorization technique. One commonly used approach is one-hot encoding, which transforms a categorical input denoted as x_{cat}, with d distinct categories, into a one-hot encoded vector $x_{cat}^{ohe} \in R^{d\times 1}$. In this encoding, the corresponding category is assigned the value 1, while all other categories are assigned the value 0 in x_{cat}^{ohe}. Moreover, the final variable, denoted as p, represents a numerical value of x_{num}. Consequently, we use a normalization procedure with the objective of centering its mean at 0 and standardizing its deviation to 1, shown as x_{num}^{norm}. This normalization step's purpose is to enhance training stability and accelerate the convergence of neural networks towards optimal solutions.

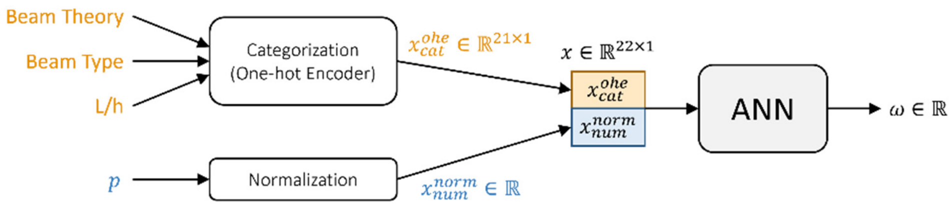

Figure 2. Input pre-processing for the ANN model.

Prior to training, the dataset is partitioned into two distinct subsets: the training dataset and the test dataset. Given the inherent susceptibility of datasets in this domain to overfit ANN models, we use dropout [23] with a rate of {0.1}. The dropout technique is commonly used for its efficacy in addressing overfitting by randomly dropping out a fraction of neurons during each training iteration.

During the training process, the model is trained on the training dataset by optimizing the model weights $\mathbf{W}$, using a loss function $f(\mathbf{W})$ that is the expected loss over the training dataset:

$$f(\mathbf{W}) = \mathbb{E}_{\xi}\left[\widetilde{f}(\mathbf{W};\xi)\right] \tag{32}$$

where ξ is a random data sample from the training dataset and $\widetilde{f}(\mathbf{W};\xi)$ is the loss function for this sample. To calculate the loss function, we use the following mean square error (MSE):

$$f(\mathbf{W}) = \frac{1}{|X|}\sum\nolimits_{i=1}^{|X|}(\overline{\omega}_i - \theta(X_i;\mathbf{W}))^2 \tag{33}$$

where X is the training dataset, $\overline{\omega}_i$ is the ground truth value for the input X_i, and $\theta(X_i;\mathbf{W})$ denotes the predicted output of the ANN model $\theta(\cdot)$, given weights W and the input X_i. The optimal solution of the problem is the following:

$$\theta(\mathbf{W}^*) = \arg_{\mathbf{W}}\min f(\mathbf{W}) \tag{34}$$

To reach this optimal solution, we optimize our model at each iteration using the following stochastic gradient descent with momentum (SGDM):

$$\theta(\mathbf{W}) = \mathbf{W} - \alpha v_{t+1} \tag{35}$$

$$v_{t+1} = \beta v_t + (1-\beta)\nabla_{\mathbf{W}} f(\mathbf{W}) \tag{36}$$

where $v_0 = 0$, α is the learning rate, and β is the momentum weight.

However, the performance of an ANN model is significantly influenced by the selection of the activation function, the number of hidden layers, their respective layer sizes, the learning rate, and the momentum weight. In order to optimize these architectural aspects, we use a grid search-based approach, systematically exploring various combinations of these hyperparameters. Our results indicate that using ReLU as the activation function, with a network depth of 3 and 35 neurons for each hidden layer, α as 0.01, and β as 0.9, yields the best performance on our dataset. For a visual representation of the final architecture of our ANN model, please refer to Figure 3.

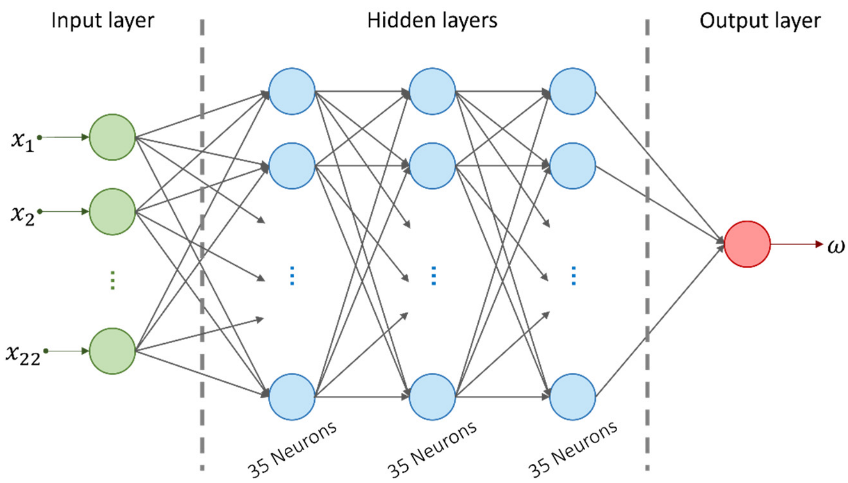

Figure 3. ANN model architecture. The set off variables from x_1 to x_{22} represent the input vector.

We implemented the ANN model using PyTorch [24]. Moreover, we designed an interface for the purpose of input provision and prediction retrieval, as illustrated in Figure 4. Then, the model was trained by the selected hyperparameters for a maximum of 300 epochs on the dataset collected from [5]. The resulting training and test losses can be seen in Figure 5. After 300 epochs, the model achieved an MSE of "0.00047" in the training dataset. Furthermore, Table 1 shows the actual and predicted frequencies for the given inputs. Through the results, the ANN model demonstrated that it predicts accurately.

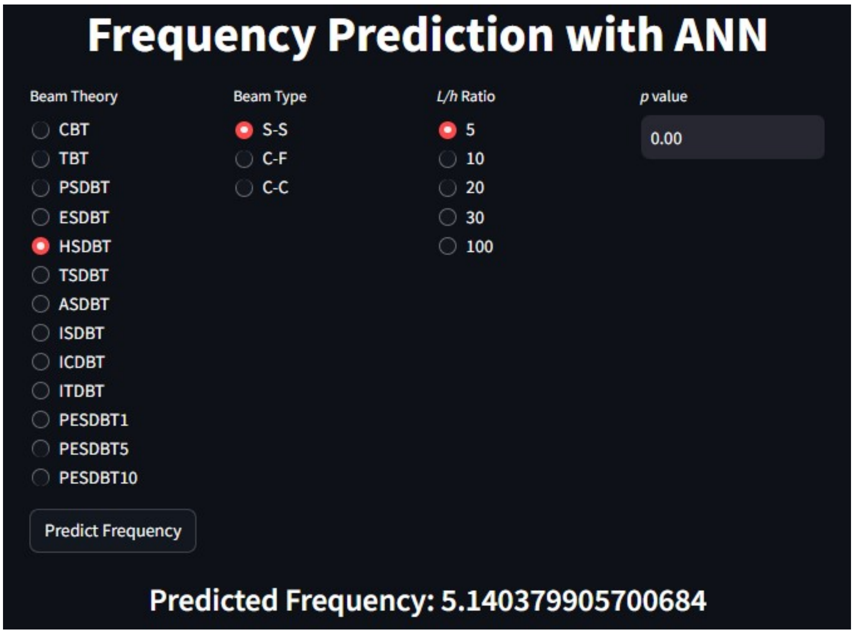

Figure 4. Interface for frequency prediction of ANN model.

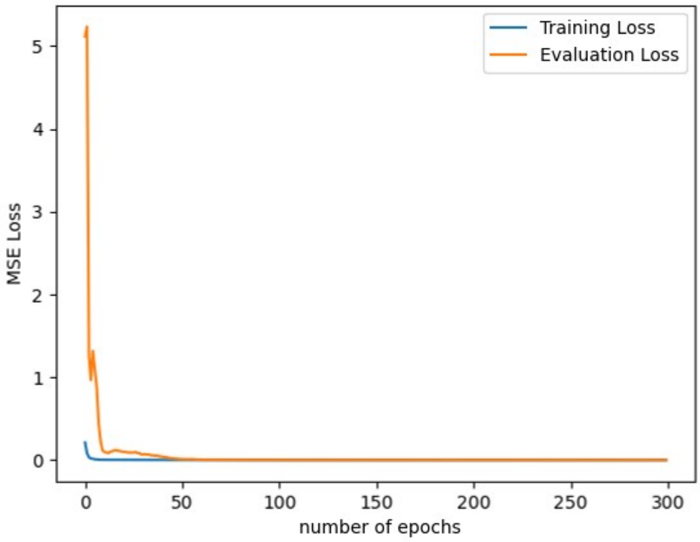

Figure 5. Training and evaluation losses through training epochs.

Table 1. Dimensionless frequencies (ϖ) of FG beams for the first mode.

Inputs				Ref. [5]	Present	ANN Prediction	Error (%)
Beam Type	Beam Theory	L/h	p				
S-S	HSDT	5	0	5.1527	5.1527	5.1404	0.24
			0.5	4.4107	4.4107	4.3784	0.73
			1	3.9904	3.9903	3.9163	1.86
			2	3.6265	3.6264	3.6419	0.42
			5	3.4014	3.4014	3.4209	0.57
			10	3.2817	3.2817	3.2072	2.27
		20	0	5.4603	5.4603	5.4503	0.18
			0.5	4.6511	4.6511	4.5956	1.19
			1	4.2051	4.2049	4.1425	1.49
			2	3.8361	3.8361	3.7991	0.96
			5	3.6485	3.6485	3.6715	0.63
			10	3.539	3.5390	3.4599	2.24

Table 1. *Cont.*

Inputs				Ref. [5]	Present	ANN Prediction	Error (%)
Beam Type	Beam Theory	L/h	p				
S-S	CBT	5	0	5.3953	5.3953	5.3703	0.46
			0.5	4.5931	4.5931	4.6144	0.46
			1	4.1484	4.1484	4.1775	0.70
			2	3.7793	3.7793	3.7545	0.66
			5	3.5949	3.5949	3.6508	1.55
			10	3.4921	3.4921	3.4816	0.30
		20	0	5.4777	5.4777	5.3975	1.46
			0.5	4.6641	4.6641	4.5927	1.53
			1	4.2163	4.2163	4.1843	0.76
			2	3.8472	3.8472	3.8234	0.62
			5	3.6628	3.6628	3.6532	0.26
			10	3.5547	3.5547	3.4890	1.85

4. Results and Discussion

In this section, the results of several numerical examples for different span-to-height (*L/h)* ratios are presented. The specific material properties of the FG beam constructed of ceramic (Al_2O_3) and metal (aluminum) in this study are given as follows:

Alumina (Al_2O_3): E_c = 380 GPa, ρ_c = 3960 kg/m^3, ν = 0.3 -aluminum (Al); E_m = 70 GPa, ρ_m= 2702 kg/m^3, ν = 0.3

The dimensional frequency can be calculated using the following formula [25]:

$$\overline{\omega} = \left(\frac{\omega L^2}{h}\right)\sqrt{\frac{\rho_m}{E_m}} \tag{37}$$

In the case of the ANN solution, the following parameters are considered as input data: span-to-height ratio, *L/h* = 5 and *L/h* = 20; beam type, simply supported (S-S), clamped-clamped (C-C), and clamped-fixed (C-F); beam theory, higher-order shear deformation beam theory or shear deformation theory (HSDBT or HSDT), CBT, TBT, ESDT, etc. (see Figure 4); and the power law varying for values 0–10. All of the results were calculated and plotted only for the HSDT and CBT in simply supported FG beams by only considering the first mode (m = 1). To validate the accuracy of the analytical method and ANN predictions, the non-dimensional frequencies (ϖ) obtained by the presented approaches were compared to a reference study conducted by Thai and Vo [5].

Table 1 indicates the comparison of non-dimensional frequency values of simply supported (S-S) FG beams for different span-to-height ratios (*L/h*), and the power law index (p) using HSDT and CBT. As can be seen from Table 1, while the value obtained with the analytical solution yields the same results as the reference study, it also converges with the ANN prediction values with a very small margin of error. These results show us the originality and quality of the trained ANN model. However, for p = 10, a higher margin of error is observed in the ANN estimation of CBT and HSDT compared to other values. The reason for this margin of error is that dimensionless natural frequency values for p = 10 for both approaches were not attained in desired level studies in the literature when the ANN dataset was created.

In order to understand the results clearly, a considerable amount of 3D and 2D diagrams (see Figures 4–12) were obtained and visualized from the analytical solution and ANN method, showing the variations of the non-dimensional frequency value according to different parameters.

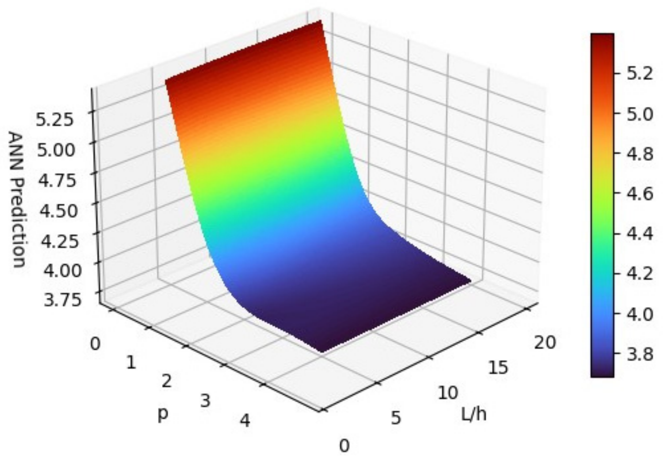

Figure 6. Non-dimensional frequency prediction ($\overline{\omega}$) of ANN for CBT.

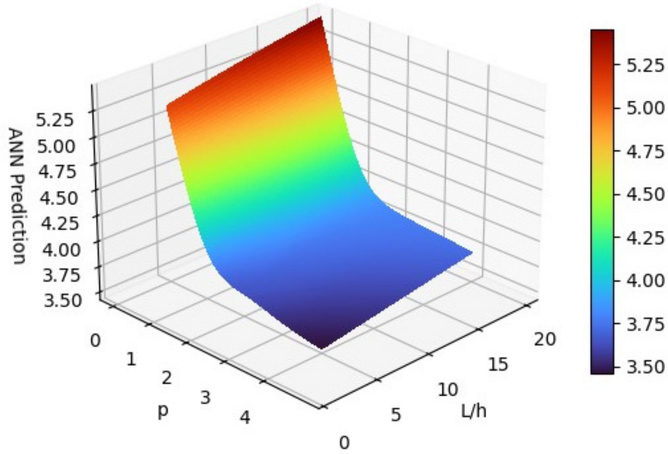

Figure 7. Non-dimensional frequency prediction ($\overline{\omega}$) of ANN for HSDT.

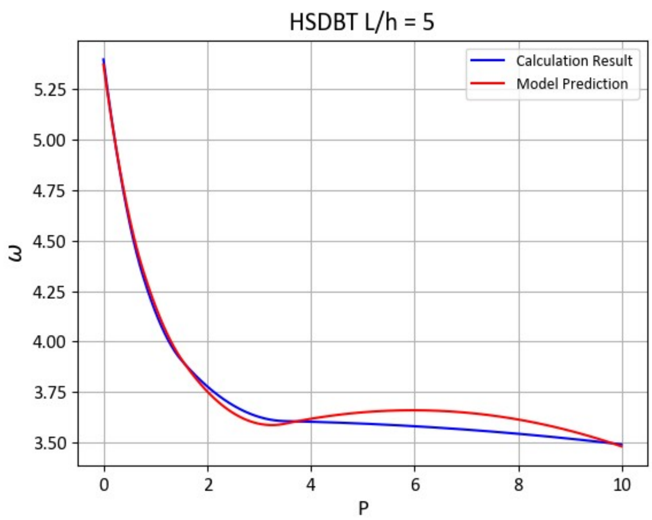

Figure 8. Non-dimensional frequency comparison obtained from HSDT and ANN for *L/h* = 5.

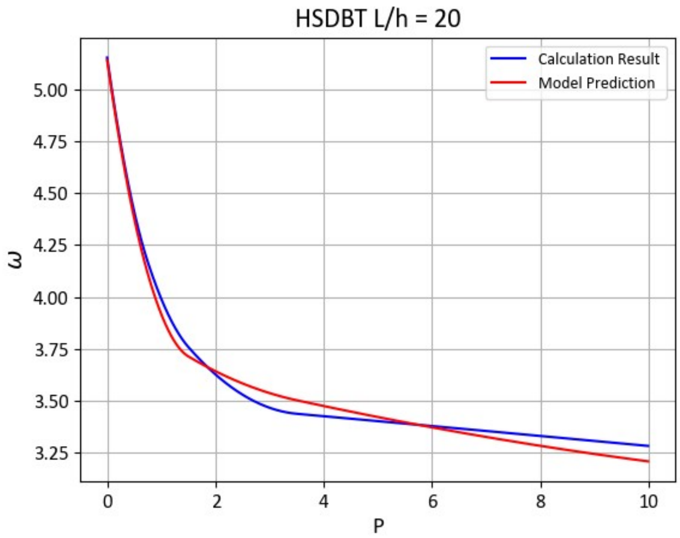

Figure 9. Non-dimensional frequency comparison obtained from HSDT and ANN for *L/h* = 20.

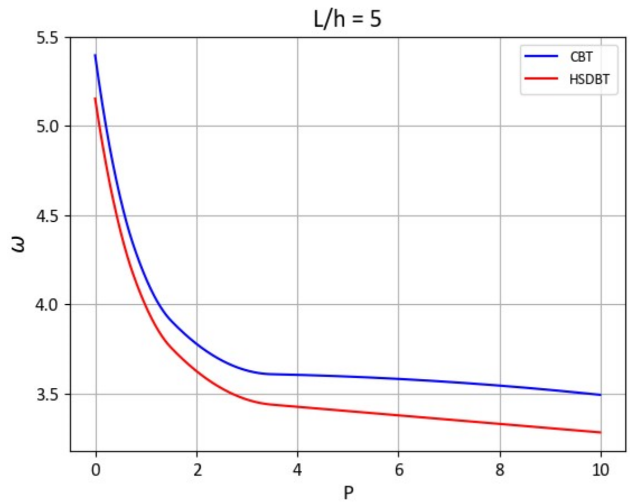

Figure 10. Non-dimensional frequency comparison obtained from CBT and HSDBT for *L/h* = 5.

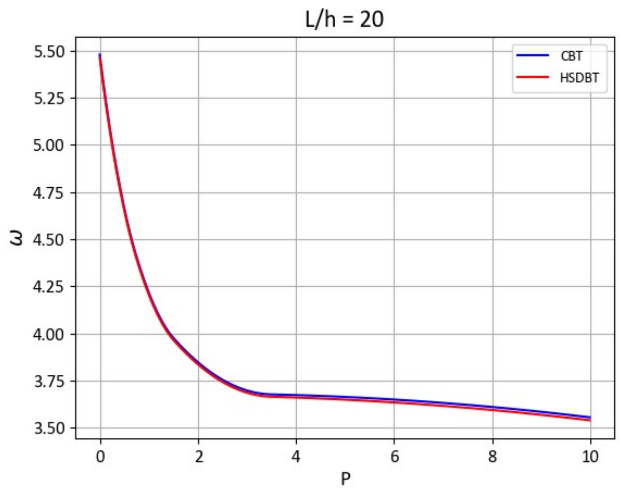

Figure 11. Non-dimensional frequency comparison obtained from CBT and HSDBT for *L/h* = 20.

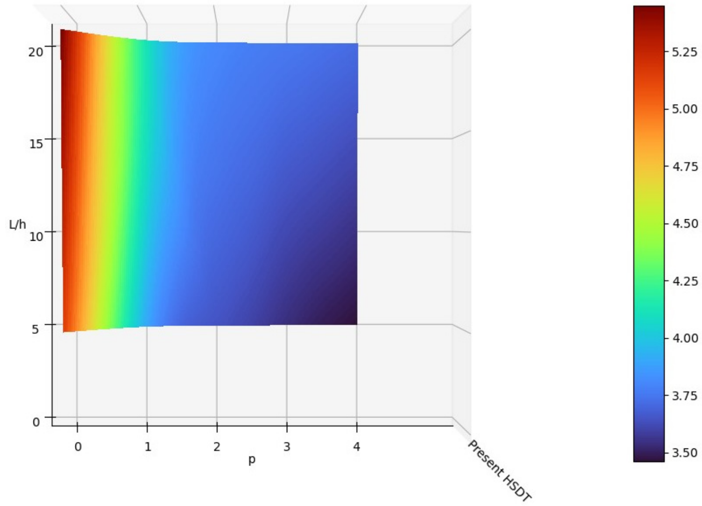

Figure 12. Values obtained from analytical solution depending on span-to-height ratio (*L/h*) and volume fraction index (*p*).

To comment on the values in the graphs, Figures 5 and 6 indicate the change of ANN prediction values according to the *L/h* ratio. As can be seen from the 3D graphics, higher frequency values were obtained for the same power law index values stemming from the increase in the span-to-height ratio. Figures 7–11 show the non-dimensional fundamental natural frequency versus the volume fraction exponent (*p*) for different values of the span-to-height ratio *L/h*. It can be understood that the lowest dimensionless frequencies are obtained for full metal ($p \to \infty$). In addition, Figure 12 demonstrates the variations in the dimensionless frequency values attained as a result of the present study that depend on the projective span-to-height ratio *L/h*.

5. Conclusions

In the present study, the free vibration of an FGM beam was analyzed via both analytical and AI approaches. To the best of the researchers' knowledge, there are limited studies in the current literature that investigate FG beams from multidisciplinary aspects. In this research, we proposed an elucidative study to represent a functionally graded material, in order to understand the vibrational behavior of those structures.

First, the FG beam was analytically solved using higher-order shear deformation theory. The governing equations were derived with the help of Hamilton's principle. The material properties were assumed vary in the thickness direction of the beam. The dimensionless frequencies for the simply supported beam were calculated by means of Navier's solution procedure. Navier's solution is an advanced solution technique that provides efficient solutions for mechanical problems. One of the main advantages of this method is that the Navier method is an important approach in terms of being adapted to solving all kinds of mechanical problems, regardless of whether 2 or 3 dimensions are involved. Considering the studies of previous research on the analysis of functionally graded structures, it has been revealed as one of the most reliable methods. Jha et al. [26] investigated the free vibration responses of functionally graded (FG) elastic, rectangular, and simply supported plates using higher-order shear deformation theories. In the study, a Navier solution technique using the double Fourier series was developed to obtain results at the desired level of accuracy, and it was emphasized that the Navier method is a suitable method for calculating the free vibration frequencies of FG plates. However, in mechanical analyses of nonlocal approaches and nonlinear functionally graded problems, Navier's method can be seen as a disadvantage in terms of being difficult to apply and not providing the desired convergence.

One can readily switch to classical beam theory (CBT) from the higher-order shear deformation theory by taking the shape function *f(z)* as zero.

Second, an artificial neural network method (ANN) was developed in order to predict the natural frequencies of FGM beams. The material properties, span-to-height ratio (L/h), power law (p), beam theory, and end conditions were provided to the ANN architecture as input data. Thus, it can be implied that the ANN method accurately represents the behavior of FGM beams.

The ANN system was trained through a dataset provided by the results of previous studies on FG beam vibrations. The analytical solution was analyzed for a higher-order shear deformation theory that considered only the first mode (m = 1) of the simply supported FG beam. Based on all of the information above, the following results were obtained:

(a) It was observed that the results obtained with HSDT substantially overlap with other higher-order shear deformation theories used in the literature.
(b) Non-dimensional frequency values obtained from the ANN converged significantly to the results obtained with the analytical solution, with a very low margin of error.
(c) The accurate natural frequency values can be attained by taking the shear effect into account (shear deformation effects lead to a decline in the natural frequencies).
(d) It can be implied that the non-dimensional frequency values obtained by higher-order shear deformation theory and classical beam theory for the analytical and ANN solutions converge depending on an increase in the span-to-height ratio.
(e) The ANN algorithm can be improved by providing more datasets to predict deformation parameters with smaller amounts of error.

The authors believe that the results listed above will be an important resource in the design of functionally graded materials that are frequently used in many fields such as energy, construction, mechanical engineering, electronics, biomedicine, aerospace, and defense.

Author Contributions: Theoretical and numerical analysis, review and editing, M.Ç.; computational research and writing, E.G.; computational research and writing, E.E.Ö.; numerical analysis and writing, E.D.; theoretical analysis, review and editing, R.A. All authors have read and agreed to the published version of the manuscript.

Funding: This research received no external funding.

Institutional Review Board Statement: Not applicable.

Informed Consent Statement: Not applicable.

Data Availability Statement: The data presented in this study are available on request from the corresponding author. The data are not publicly available due to privacy.

Conflicts of Interest: The authors declare no conflict of interest.

References

1. Reddy, J.N. A simple higher-order theory for laminated composite plates. *J. Appl. Mech.* **1984**, *51*, 745–752. [CrossRef]
2. Yesilce, Y.; Catal, H.H. Solution of free vibration equations of semi-rigid connected Reddy–Bickford beams resting on elastic soil using the differential transform method. *Arch. Appl. Mech.* **2011**, *81*, 199–213. [CrossRef]
3. Touratier, M. An efficient standard plate theory. *Int. J. Eng. Sci.* **1991**, *29*, 901–916. [CrossRef]
4. Soldatos, K. A transverse shear deformation theory for homogeneous mono-clinic plates. *Acta Mech.* **1992**, *94*, 195–220. [CrossRef]
5. Thai, H.T.; Vo, T.P. Bending and free vibration of functionally graded beams using various higher-order shear deformation beam theories. *Int. J. Mech. Sci.* **2012**, *62*, 57–66. [CrossRef]
6. Pham, Q.H.; Tran, T.T.; Nguyen, P.C. Nonlocal free vibration of functionally graded porous nanoplates using higher-order isogeometric analysis and ANN prediction. *Alex. Eng. J.* **2023**, *66*, 651–667. [CrossRef]
7. Reddy, J. Analysis of functionally graded plates. *Int. J. Numer. Methods Eng.* **2000**, *47*, 663–684. [CrossRef]
8. Vel, S.S.; Batra, R.C. Exact solution for thermoelastic deformations of functionally graded thick rectangular plates. *AIAA J.* **2002**, *40*, 1421–1433. [CrossRef]
9. Ferreira, A.J.M.; Batra, R.C.; Roque, C.M.C.; Qian, L.F.; Martins, P.A.L.S. Static analysis of functionally graded plates using third-order shear deformation theory and a meshless method. *Compos. Struct.* **2005**, *69*, 449–457. [CrossRef]
10. Neves, A.M.A.; Ferreira, A.J.M.; Carrera, E.; Roque, C.M.C.; Cinefra, M.; Jorge, R.M.N.; Soares, C.M.M. A quasi-3D sinusoidal shear deformation theory for the static and free vibration analysis of functionally graded plates. *Compos. B. Eng.* **2012**, *43*, 711–725. [CrossRef]

11. Taj, M.G.; Chakrabarti, A.; Sheikh, A.H. Analysis of functionally graded plates using higher order shear deformation theory. *Appl. Math. Model* **2013**, *37*, 8484–8494.
12. Li, X.F. A unified approach for analyzing static and dynamic behaviors of functionally graded Timoshenko and Euler-Bernoulli beams. *J. Sound Vib.* **2008**, *318*, 1210–1229. [CrossRef]
13. Huang, Y.; Li, X.F.A. New approach for free vibration of axially functionally graded beams with non-uniform cross-section. *J. Sound Vib.* **2010**, *329*, 2291–2303. [CrossRef]
14. Aydogdu, M.; Taskin, V. Free vibration analysis of functionally graded beams with simply supported edges. *Mater. Des.* **2007**, *28*, 1651–1656. [CrossRef]
15. Mahi, A.; Bedia, E.A.A.; Tounsi, A.; Mechab, I. An analytical method for temperature-dependent free vibration analysis of functionally graded beams with general boundary conditions. *Compos. Struct.* **2010**, *92*, 1877–1887. [CrossRef]
16. Sankar, B.V. An elasticity solution for functionally graded beams. *Compos. Sci. Technol.* **2001**, *61*, 689–696. [CrossRef]
17. Zhang, D.G.; Zhou, Y.H. A theoretical analysis of FGM thin plates based on physical neutral surface. *Comput. Mater. Sci.* **2008**, *44*, 716–720. [CrossRef]
18. Shahrjerdi, A.; Bayat, M.; Mustapha, F.; Sapuan, S.; Zahari, R. Second-order shear deformation theory to analyze stress distribution for solar functionally graded plates. *Mech. Based Des. Struct. Mach.* **2010**, *38*, 348–361. [CrossRef]
19. Demirkan, E.; Artan, R. Buckling analysis of nanobeams based on nonlocal Timoshenko beam model by the method of initial values. *Int. J. Struct. Stab. Dyn.* **2018**, *19*, 1950036. [CrossRef]
20. Çelik, M.; Artan, R. An investigation of static bending of a bi-directional strain-gradient Euler–Bernoulli nano-beams with the method of initial values. *Microsyst. Technol.* **2020**, *26*, 2921–2929. [CrossRef]
21. Çelik, M.; Artan, R. Buckling Analysis of a Bi-Directional Strain-Gradient Euler–Bernoulli Nano-Beams. *Int. J. Struct. Stab. Dyn.* **2020**, *20*, 2050114. [CrossRef]
22. Larbi, O.L.; Kaci, A.; Houari, M.S.A.; Tounsi, A. An Efficient Shear Deformation Beam Theory Based on Neutral Surface Position for Bending and Free Vibration of Functionally Graded Beams. *Mech. Based Des. Struct. Mach.* **2013**, *41*, 421–433. [CrossRef]
23. Srivastava, N.; Hinton, G.; Krizhevsky, A.; Sutskever, I.; Salakhutdinov, R. Dropout: A simple way to prevent neural networks from overfitting. *J. Mach. Learn. Res.* **2014**, *15*, 1929–1958.
24. Paszke, A.; Gross, S.; Massa, F.; Lerer, A.; Bradbury, J.; Chanan, G.; Chintala, S. Pytorch: An imperative style, high-performance deep learning library. In *Advances in Neural Information Processing Systems*; Institute of Electrical and Electronics Engineers (IEEE): Piscataway, NJ, USA, 2019; Volume 32.
25. Zohra, Z.; Lemya, H.; Abderahman, Y.; Mustapha, M.; Abdelouahed, T.; Djamel, O. Free vibration analysis of functionally graded beams using a higher-order shear deformation theory. *Math. Model. Eng. Probl.* **2017**, *4*, 7–12. [CrossRef]
26. Jha, D.K.; Kant, T.; Singh, R.K. Free vibration response of functionally graded thick plates with shear and normal deformations effects. *Compos. Struct.* **2012**, *96*, 799–823. [CrossRef]